

STEADY AERODYNAMIC SIMULATION OF A HIGH-LIFT GEOMETRY BY MEANS OF A HYBRID EULER/INTEGRAL BOUNDARY LAYER CODE

Daniel Sampaio Souza, dss-em@usp.br

Marcello Augusto Faraco de Medeiros, marcello@sc.usp.br

University of São Paulo, São Carlos, Brazil.

Abstract. *The flowfield around multi-element airfoils is very complex. An accurate characterization of these flowfields is necessary to precisely predict high-lift wing properties like drag and aeroacoustic behavior. In this matter the transition locations of the boundary layers (BL) play a significant roll, since they dictate the thickness of the shear layers. Traditional Computational Fluid Dynamic (CFD) codes do not have reliable algorithms to predict transition. Common high-lift CFD models consider either fully turbulent flows or transition locations given by expensive wind tunnel experiments. This work simulates the bidimensional flow over a high-lift geometry under flight Reynolds number regime in angles of attack between 8 and 18 degrees with an hybrid Euler/Integral Boundary Layer (Euler/IBL) code. The code used is the MSES by Mark Drela, developed to calculate flows over multi-element airfoils for both analysis and design proposes. It is a hybrid code that solves the Euler equation with corrections to the BL and wakes calculated by integral methods. Transition locations are predicted with a simplified form of the e^n algorithm. Comparison of the results with experimental data available on the literature will assess the accuracy of the code in calculating aerodynamic parameters that are important to aeroacoustic related phenomena, like drag and transition locations. The studied geometry is a three-element high-lift airfoil created by McDonnell Douglas and named in the literature as 30P30N. It consists of a leading-edge slat, a main element and a single flap. Polar curves are compared to experimental results as well as the transition locations to determine the parameters that better simulate the wind tunnel conditions. Discrepancies between experiments and computations are observed in the pressure distribution. Lift coefficient are predicted with an error of 6.3% relative to experimental result for 18 degrees configuration and drag has an error of 40.3% at 16 degrees and 17.9% at 8 degrees. Despite the differences in C_p distribution transition is predicted according to measurements in both surfaces of main element and flap suction side.*

Keywords: *aerodynamic, transition, high-lift, integral boundary layer*

1. INTRODUCTION

The noise generated by a commercial aircraft is commonly separated in two components depending on the sources, the engine noise and the airframe noise. During the take-off procedure, when high thrust is required, the engine noise overlays all the others. But with the employment of elevate by-pass ratio turbo-fans in jetliners, the airframe noise suffered a growth in importance, mainly in approach and landing situations (Dobrzynski et al. 2008).

The most important components related to airframe noise are the landing-gear and the high-lift devices. The landing gears have very non-aerodynamic shape that causes massive separation of the BL's and a wake with high level of turbulence. In a general high-lift system the noise is generated by flow unsteadiness in the cavities and by three-dimensional features in its geometry. A typical spectrum of noise generated in the slat region has broadband component of low and mid-frequencies and a tonal peak of high frequency (Khorrami et al. 2003).

An accurate prediction of aeroacoustic noise by means of computational tools depends on a good solution of the transient flow. Meredith (1993 *apud* Rumsey et al., 1998) points the transition of the BL, the interaction between shock and BL, wake-BL confluence and BL separation as important features of the flow over high-lift airfoils. So the proper simulation of these phenomena might be the key for a good solution of high-lift's time-dependent aerodynamic. Several works have concerned in well characterize the flow dynamics in the slat cove region. After previous fully turbulent time-accurate simulations Khorrami *et al.* (2001) employed an excitation of the BL upstream of the slat cusp in order to overcome the high artificial dissipation caused by the numerical model and capture large scale structures of the free shear layer that were being damped in earlier calculations. The result showed the structures but the acoustic analysis was affected by the induced excitation. Also with the purpose to minimize the damping effect Khorrami *et al.* (2002) propose a different approach. They turned off the production term of the URANS turbulence model in the slat cove area. The modification was likewise successful in capturing the flow structures but without the undesired influence on the acoustic calculation. In two complementary works Jenkins *et al.* (2004) and Khorrami *et al.* (2004) compare the result of 2D time-accurate computation in the slat region with PIV images. Overall good agreement was achieved for the averaged velocity and vorticity fields but the large scale structures of the shear layer were excessively energized in the CFD calculations. To test the conjecture that the discrepancy in the development of the shear layer was caused by unconsidered 3D effects, Choudhari & Khorrami (2006) carried out a quasi-3D CFD simulation of the same airfoil as Jenkins *et al.* (2004) and Khorrami *et al.* (2004). The solution compared better to PIV analysis then the previous 2D calculation, indicating that the more unstable behavior was in fact related to the absence of consideration of 3D

phenomena. Rumsey *et al.* (1998) exhibit improvements in results of numerical simulations of high-lift system when the locations of the BL transition are taken into account. They set up the CFD model according to experimental results of transition and compare the velocity profile over the upper surfaces of the main element and flap with experiment and fully turbulent calculations. Klausmeyer & Lin (1994) show also show improvement in CFD results of high-lift system by imposing the BL transition locations on the simulations. They compare results of C_f with measurements from both fully-turbulent and transition considering calculations.

The present work tests the hybrid Euler/IBL code MSES. To carry out the tests numerical results of the pressure coefficient, of the force coefficients (C_d and C_l), and of the locations of BL transition are compared with experimental results present in the literature. The transition locations predicted with the hybrid code are meant to be used as input in simulations with traditional CFD codes in future works. A range of values for critical n are employed to determine the value that better simulate the conditions on the tunnel. Also C_d and C_l are compared with results of similar simulations. A brief description of the computational code is presented in section 2. In the section 3 the studied geometry and the considered flow conditions are presented. The section 4 presents the numerical results and the comparison with experiments and other numerical efforts and the section 5 closes with the final considerations.

2. MSES CODE

MSES is a hybrid code that solves the Euler equation in the steady state form at the regions of potential flow and applies Integral Boundary Layer (IBL) methods to solve the flow on viscous regions, such as boundary layers and wakes. The coupling between the potential and viscous flows is made through the displacement thickness. The Euler equations in conservative form are discretized with a finite volume formulation using an upwind scheme.

The domain where the Euler equations are solved is discretized by a structured grid based on the streamlines. So the finite volumes are limited by streamlines at the upper and lower bounds (see Fig. 1). With this form of discretization there is no transport of mass between control volumes separated by streamlines and the convection occurs only in two surfaces of the cell. A great advantage brought by this form of space discretization is the reduction of the number of equations to be solved. The continuity and energy equations can be replaced respectively by the considerations of constant flux and constant stagnation enthalpy along the streamtube. With these considerations the number of variables at a node reduces from four to two, and further considerations regarding the pressure exchanged by two tubes permits the number of variables to fall to one per node (Drela 2006). So the discretized momentum equation assumes the form

$$\Delta p + \frac{m}{A} \Delta \tilde{q} - P_s = 0 \quad (1)$$

The term P_s in Eq. (1) represents a correction that take into account the pressure at the streamlines limiting the finite volume at upper and lower bounds. The variations Δ are carried through the streamtube. The term \tilde{q} is the modified velocity that encloses artificial dissipation to enable capturing of shock.

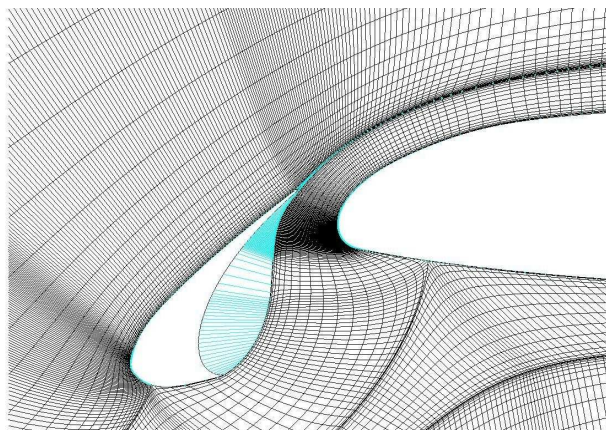


Figure 1. MSES grid in the region slat cove.

Commonly hybrid codes start the calculation with the potential solution, use its result as input to solve the BL equations and apply the displacement thickness d^* to define a new geometry used to solve the potential equations of the next iteration. This process repeats until the solution converges. Different from traditional hybrid codes, MSES couples the potential and viscous equations in one system of non-linear equations and solve them together through a Newton method (Drela 2006). This method causes MSES solution to converge more rapidly but on the other side it requires a

good initial guess. The prediction of transition location is carried using a simplified form of the e^n method. It determines the amplitude of most amplified Tollmien-Schlichting frequency in each point of the surface (Drela 2006).

3. 30P30N GEOMETRY AND NUMERICAL MODEL

Figure 2 shows the 2D wing profile used in the present study. It is a three-element airfoil with a leading-edge slat, a main element and a single trailing-edge flap. The slat and flap chords are, respectively, 14.48% and 30% of the chord of the stowed airfoil. The configuration of the high-lift devices are showed in Tab. 1. The values are percentages of the stowed chord. This airfoil is known in the literature as MD 30P30N, was developed by McDonnell Douglas and is largely documented with both experimental and numerical results, which is the reason why it was chosen to the present study.



Figure 2. Airfoil MD 30P30N.

Table 1. Geometric configurations of airfoil MD 30P30N

	SLAT	FLAP
GAP	2.95%	1.27%
OVERHANG	-2.5%	0.25%
ANGLE	30°	30°

The flow condition employed in the numerical calculations considers a Mach number of 0.2 and Reynolds number of 9 millions. This condition was chosen to match the conditions with transition location documented by Bertelrud (1998). This configuration is representative of the conditions of a real commercial aircraft in landing procedure. The simulations consider that the airfoil is placed inside a wind tunnel by assuming free-slip wall boundary conditions on the upper and lower bounds of the simulation domain. The distance between the walls takes into account the geometry of the NASA’s Low Turbulence Pressure Tunnel (LTPT) at Langley. The position of the inlet and outlet boundary conditions was defined by a study of domain convergence. This study ensures that the responses are independent of size of the domain.

4. RESULTS AND DISCUSSIONS

In this section the results of the numerical analysis performed with the MSES code are presented including comparison with experimental results and computations from other hybrid code users.

4.1. Grid Convergence Study

To demonstrate the independence of the results relative to the used spatial discretization, a grid convergence study was carried out. The test compared four different meshes, that are described in Tab. 2. The coordinate “I” refers to the direction of the flow while coordinate “J” refers to the direction normal to the flow. The refinement ratio between the finest and the coarsest meshes is equal to 1.49 in the coordinate I and 1.57 in coordinate J.

Figures 3 and 4 show the values of lift and drag coefficient for the four studied meshes with the 8 degrees angle of attack configuration. It can be seen that the drag is almost insensible to grid refinement for the tested meshes. On the other hand C_l presents a more significant variation. However, even the lift coefficient is very stable in grids so refined as grid 3 and 4. Comparing those two grids the variation in C_d and C_l is of 0.16% which corresponds to an acceptable convergence of the mesh. Similar studies were made to the other values of angle of attack to ensure grid independence.

Table 2. Grid configurations tested in the convergence study.

GRID	I	J	NR. OF CELLS
1	306	49	14994
2	373	60	22380
3	411	69	28359
4	455	77	35035

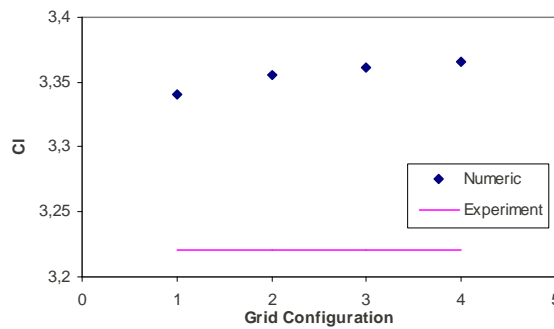


Figure 3. Lift coefficient for the four grids tested.

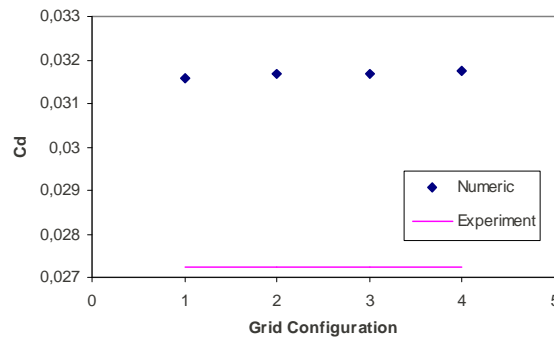


Figure 4. Drag coefficient for the four grids tested.

4.2. Pressure Distribution

In Fig. 5, Fig. 6 and Fig. 7, the numerical result of C_p distribution over the surfaces of the three elements are compared with measurements presented by Bertelrud (1998) for a configuration of 8 degrees angle of attack. The scale of the horizontal axis is the length along the surface non-dimensionalized by the stowed chord of the airfoil. Figure 5 show a significant discrepancy between simulation and experiment on the slat's upper surface. The calculated result has two points of elevated suction level while the experiment shows only one suction peak. The C_f distribution presents no negative value in this region indicating that the unusual behavior of the C_p curve is not related to the presence of a laminar separation bubble. On the main element and flap the suction peak occurs at a location upstream of the measured position and is more intense as shown in Fig. 6 and Fig. 7. On the lower surface of the main element the flow experiences a favorable pressure gradient until s/c approximately equal to -0.45 where the gradient becomes unfavorable. This adverse pressure gradient is more intense in the experiment than in the numerical simulation. Another difference lies on the step-like suction recover on the main element upper surface. Although this feature is present in both calculations and experiment they are placed in different location along the surface. On the lower surface of the flap the numerical and experimental curves collapse.

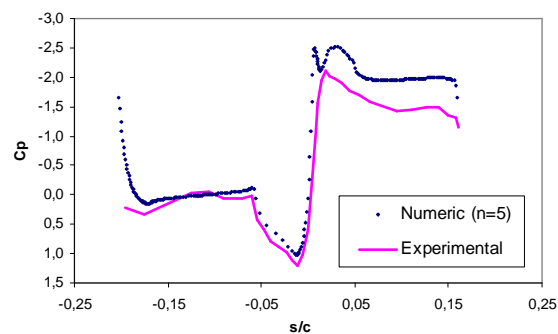


Figure 5. C_p distribution over the slat surface for 8° AOA.

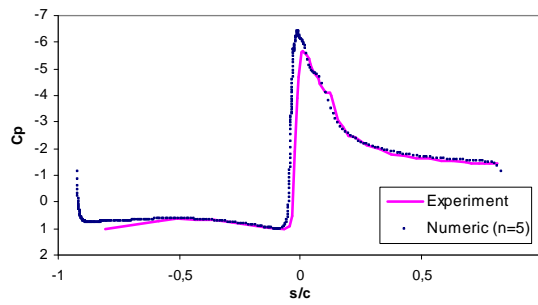


Figure 6. C_p distribution over the main element surface for 8° AOA.

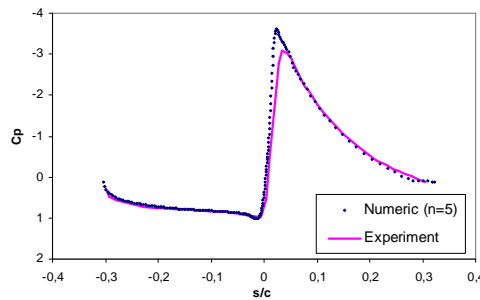


Figure 7. C_p distribution over the flap surface for 8° AOA.

For 16 degrees angle of attack (Fig. 8, 9 and 10), the slat's suction peak is predicted more intense and more upstream in comparison to the experiment of Bertelrud (1998), but good agreement is achieved in the rest of the suction side and on the pressure side. In this configuration the main element and the flap have very similar features. Comparing both to the 8 degrees configuration, the suction peaks are still calculated upstream of the measured location but their level are in better accordance with experiments for 16 degrees angle of attack. Also the area under the curve has grown more in the experiment than in computations relative to the 8 degrees configuration. Good agreement between calculations and experiment is achieved in lower surface of both elements.

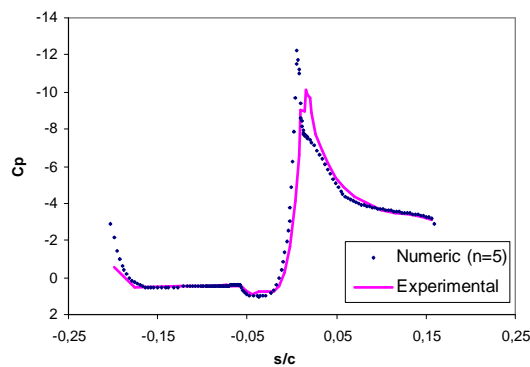


Figure 8. C_p distribution over the slat surface for 16° AOA.

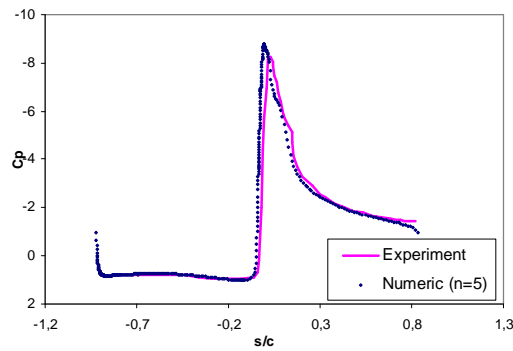


Figure 9. C_p distribution over the main element surface for 16° AOA.

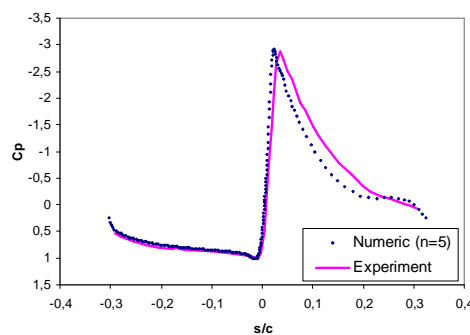


Figure 10. C_p distribution over the flap surface for 16° AOA.

4.3. Lift and Drag Coefficients

Figure 11(a) presents the lift coefficient values measured by Spaid & Lynch (1996) with angle of attack spanning from 8 degrees to 18 degrees together with the calculated values considering a critical n range between 4 and 9. Analyzing the effect of changing the critical n , one can see that it has little influence on the C_l value over the range of α considered. This means that the range of n studied is not sufficient to cause a variation of the BL thicknesses that is significant to the lift coefficient. Comparing the behavior of the numerical and experimental curves one can see that the numerical model does not represent well the effect of angle of attack variation. The experimental curve is almost linear in the studied range of α , while the numeric one presents a downward concavity so that the C_l values are over-predicted for angles of attack below 12 degrees and under-predicted for angles beyond 12 degrees. This observation is in agreement with variation of C_p distribution caused by the increase in attitude. If we look to the lift generated by each element (not shown here) the same trend is observed in each one of them as in the total lift curves, which indicate that no element alone is responsible for the difference between experiment and calculations. The drag polar in Fig. 11(b) shows that calculated drag is greater than the measured for all values of α and critical n considered. It is also clear that the value of critical n has more relative influence on drag than in lift coefficient.

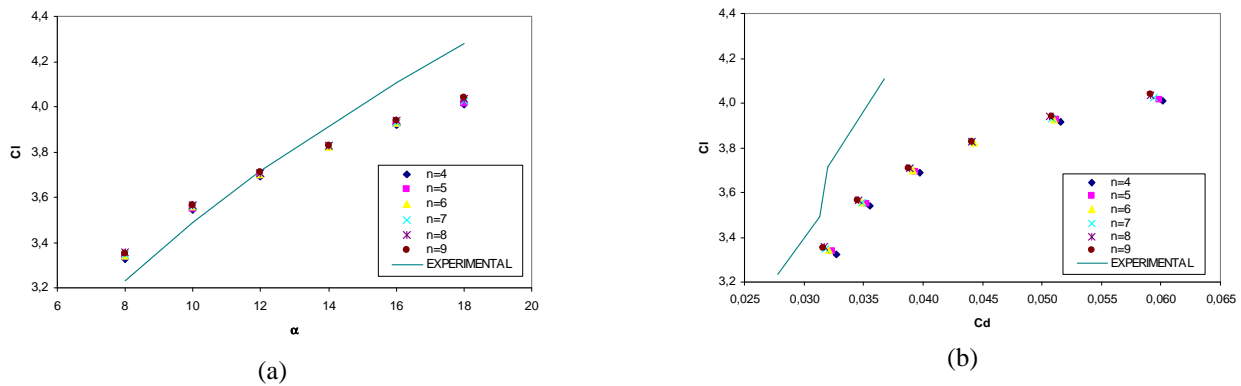


Figure 11. Graphics of (a) C_l and (b) C_d of the simulation results compared with experiments.

Comparing the present results for lift and drag coefficient with results from other hybrid codes for the same case, presented in the Fig. 3(a) of Klausmeyer & Lin (1997), the present results compare better with the experimental curve of lift than most of the others in absolute values, but it has the worst performance in imitating the curve slope in the linear region. Regarding to drag prediction the present simulation performs as good as others' best ones for the lower angles of attack but presents decay in quality for high angles of attack.

4.4. Transition Locations

In this section the transition locations predicted by the simplified form of the e^n method are compared with experimental results found in the literature. For the slat and flap only the transition on the upper surface is addressed, since the BL is laminar in the slat lower surface until it separates in the cusp and in the entire flap lower surface for all considered configurations in both experiment and computations. Also the results of some combinations of critical n and angle of attack are missing (e.g. 14 degrees with n equal to 4 and 5). For these configurations the solution did not converged although some attempts have been made starting with converged solution of close configurations. The experimental results were measured by Bertelrud (1998) that reports the start and end location of the transition process in each case.

Slat

Figure 12 shows transition locations of the BL over the upper surface of the slat. The different marks are the numerical results for all the critical n 's considered. For the 8 degrees configuration the predicted position is within the measured region for all evaluated values of n despite the big difference in the C_p distribution. As the angle of attack increases the transition is predicted earlier than the measured start location and becomes almost independent of the critical n . This behavior is consequence of the stronger calculated suction peak (see Fig. 8) that causes a laminar separation that doesn't happen in the experiments. Laminar separation on slat of 30P30N geometry in disagreement with experiments is also reported by Rumsey (1998) in numerical simulation with a traditional CFD code that considers the transition location, but only for 19 degrees angle of attack.

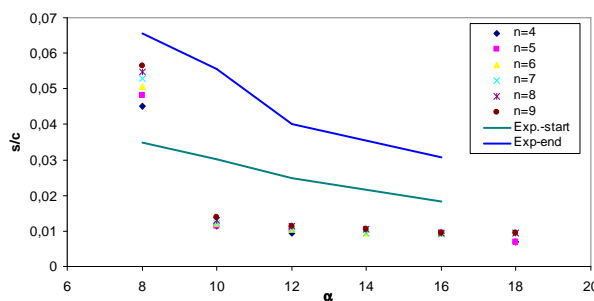


Figure 12. Numerical and experimental results of transition location on slat upper surface.

Main Element

The predicted transition location on the main element suction side is showed at Fig. 13 together with experimental measurements. Except for 8 degrees angle of attack only the results of the models with small value of n inside the

measured region, basically n equal to 4 and 5. Again despite the great difference between the calculated and measured distribution of pressure the code was able to predict the transition in reasonable accordance with experiments. The results for the lower surface are presented on Fig. 14. From the 12 degrees configuration on the BL reaches the cusp and separates before the end of transition process. Although the prediction for 10 and 12 degrees lies in the measured region the transition is predicted later in comparison to experiment when the airfoil is at 8 degrees angle of attack. This corroborates the discrepancy in pressure distribution, since the computed C_p curve presents a milder adverse gradient on the lower surface of the main element (see Fig. 6).

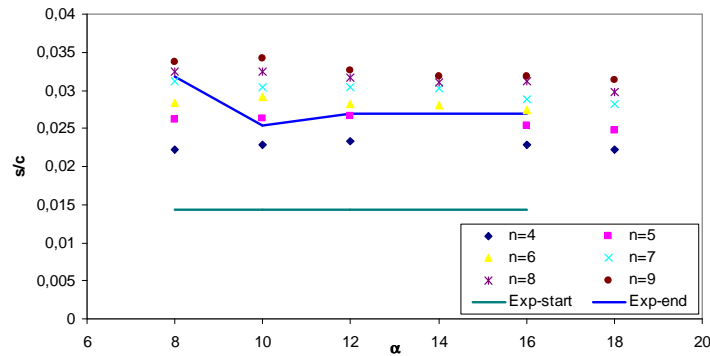


Figure 13. Numerical and experimental results of transition location on main element upper surface.

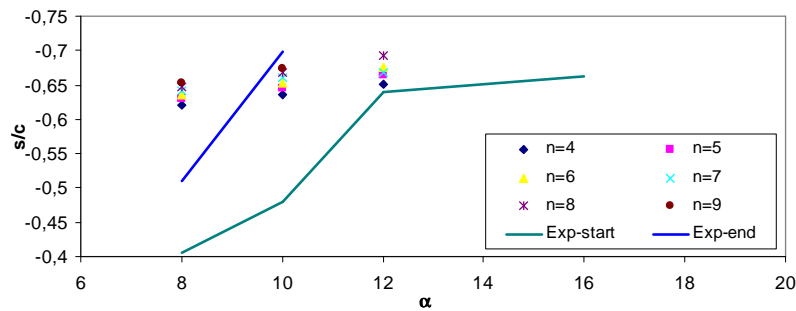


Figure 14. Numerical and experimental results of transition location on main element lower surface.

Flap

As can be seen in Fig. 15 almost all considered configuration that was simulated agreed with the measured locations. However the computed results show a tendency of the transition location to move upstream as the angle of attack increases, while the experiment exhibits a practically constant central region with little variations on start and end points. Looking at the computed variation in C_p distribution on the suction side of the flap caused by increasing angle of attack we see that although the suction peak intensity comes closer to the measured value, the pressure gradient becomes more adverse in the numerical simulation. This behavior may explain the relation between predicted transition location and angle of attack.

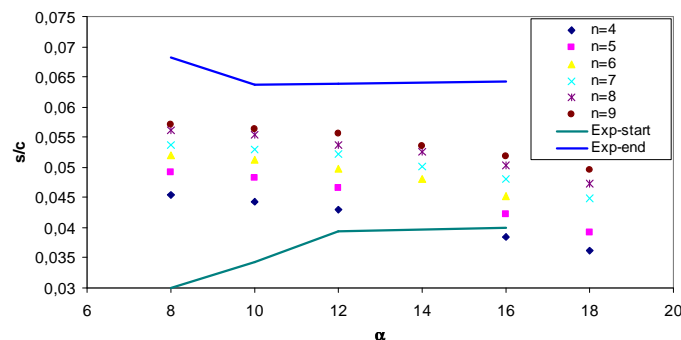


Figure 15. Numerical and experimental results of transition location on flap upper surface.

5. CONCLUSIONS

Bidimensional simulations of the 30P30N geometry were carried out using the hybrid Euler/IBL code MSES. The wind tunnel's floor and ceiling were considered as free-slip walls and imitates the dimensions of the NASA LTPT at Langley. The simulation results were compared to experimental reports and computations from other hybrid codes for the same geometry to assess the accuracy of the model to predict the transition location of the BL. The noteworthy conclusions of the present study are listed below.

- Systematic discrepancy is observed on the distribution of C_p over the three elements;
- The value of n critical has small influence on the calculated values of C_l and C_d ;
- The model's results for C_l are comparable with the results from other hybrid codes in values but the relation between C_l and angle of attack is not as good captured;
- The C_d results close the results from others hybrid code for moderate angles of attack but predict much more wrong drag than the best ones at higher attitudes;
- Despite the differences between the predicted and measured pressure distributions the model were capable to accurately predict the transition locations in most of the configurations except on the slat upper surface because of an unrealistic captured laminar separation;
- The differences in the C_p distribution don't enable a proper conclusion about the values of n that better simulates the conditions inside the tunnel.

6. REFERENCES

- Bertelrud, A., 1998, "Transition on a Three-Element Configuration at High Reynolds Numbers", AIAA Paper 98-0703.
- Choudhari, M., Khorrani, M.R., 2006, "Slat Cove Unsteadiness: Effect of 3D Flow Structures", 44th AIAA Aerospace Sciences Meeting and Exhibit, AIAA 2006-0211, Reno, United States.
- Dobrzynski, W., Ewert, R., Pott-Pollenske, M., Herr, M., Delfs, J., 2008, "Research at DLR Towards Airframe Noise Prediction and Reduction", Aerospace Science and Technology, Vol. 12, No. 1, pp. 80-90.
- Drela, M., 2006, "A User's Guide to MSES 3.04", MIT Department of Aeronautics and Astronautics.
- Jenkins, L.N., Khorrani, M.R., Choudhari, M., 2004, "Characterization of Unsteady Flow Structures Near Leading-Edge Slat: Part I. PIV Measurements", 10th AIAA/CEAS Aeroacoustic Conference, AIAA 2004-2801, Manchester, Great Britain.
- Khorrani, M.R., Choudhari, M., Jenkins, L.N., 2004, "Characterization of Unsteady Flow Structures Near Leading-Edge Slat: Part II. 2D Computations", 10th AIAA/CEAS Aeroacoustic Conference, AIAA 2004-2802, Manchester, Great Britain.
- Khorrani, M.R., Choudhari, M., Singer, B.A., Lockard, D.P., Streett, C.L., 2003, "In Search of the Physics: The Interplay of Experiment and Computation in Slat Aeroacoustics", 41st Aerospace Sciences Meeting & Exhibit, AIAA 2003-0980, Reno, United States.
- Khorrani, M.R., Singer, B.A., Berkman, M.E., 2001, "Time-Accurate Simulations and Acoustics Analysis of Slat Free-Shear Layer", AIAA 2001-2155.
- Khorrani, M.R., Singer, B., Lockard, D., 2002, "Time-Accurate Simulations and Acoustics Analysis of Slat Free-Shear-Layer: Part II", 8th AIAA/CEAS Aeroacoustic Conference & Exhibit, AIAA 2002-2579, Breckenridge, United States.
- Klausmeyer, S.M., Lin, J.C., 1994, "An experimental Investigation of Skin Friction on a Multi-Element Airfoil", 12th AIAA Applied Aerodynamics Conference, AIAA 94-1870, Colorado Springs, United States.
- Klausmeyer, S.M., Lin, J.C., 1997, "Comparative Results from a CFD Challenge Over a 2D Three-Element High-Lift Airfoil", NASA Technical Memorandum 112858, Hampton, United States.
- Rumsey, C.L., Gatski, T.B., Ying, S.X., Bertelrud, A., "Prediction of High-Lift Flows Using Turbulent Closure Models", 1998, AIAA Journal, Vol. 36, No. 5, pp. 765-774.
- Spaid, F.W., Lynch, F.T., 1996, "High Reynolds Number, Multi-Element Airfoil Flowfield Measurements", AIAA 34th Aerospace Sciences Meeting and Exhibit, AIAA Paper 96-0682, Reno, United States.

7. RESPONSIBILITY NOTICE

The authors are the only responsible for the printed material included in this paper.